ISH Journal of Hydraulic Engineering

ISSN: 0971-5010 (Print) 2164-3040 (Online) Journal homepage: http://www.tandfonline.com/loi/tish20

Geometry effect and generalization of velocity distribution in asymmetric compound channels

Issam A. Al-Khatib & Mustafa Gogus

To cite this article: Issam A. Al-Khatib & Mustafa Gogus (2014) Geometry effect and generalization of velocity distribution in asymmetric compound channels, ISH Journal of Hydraulic Engineering, 20:3, 301-313, DOI: 10.1080/09715010.2014.902171

To link to this article: http://dx.doi.org/10.1080/09715010.2014.902171

Published online: 04 Apr 2014.

ISH Journal of Hydraulic Engineering, 2014
Vol. 20, No. 3, 301–313, http://dx.doi.org/10.1080/09715010.2014.902171

Taylor & Francis
Taylor & Francis Group

Geometry effect and generalization of velocity distribution in asymmetric compound channels

Issam A. Al-Khatib[a]* and Mustafa Gogus[b]

[a]*Institute of Environmental and Water Studies, Birzeit University, Birzeit, Palestine;* [b]*Hydraulics Division, Civil Engineering Department, Middle East Technical University, Ankara, Turkey*

(*Received 14 August 2013; accepted 18 February 2014*)

Nine different geometries with asymmetric rectangular compound cross-sections were tested in a laboratory flume in order to investigate effects of the geometry on the values of three different dimensionless velocity ratios. A generalized single variable regression model has been derived to predict each of the three dimensionless velocity ratios with high accuracy. Another set of the multiple-variable regression models has been derived using one additional dimensionless parameter which is the ratio of the upstream channel width to the main channel width. The application of several key statistics and validation procedures has indicated that the developed models predict the three mean dimensionless velocity ratios with high correlation coefficients.

Keywords: asymmetric compound channel; geometry; floodplain; main channel; velocity distribution

1. Introduction

In water resources planning, engineering practice, dredging the main channel, and lowering or smoothing floodplains involve overbank flow. Therefore, there is great theoretical application value and significance in studying overbank flow (Al-Khatib et al. 2013; Yang et al. 2010).

Information regarding the nature of velocity and flow distribution in simple and compound channels is needed to solve a variety of river hydraulics and engineering problems. The flow distribution, velocity distribution and flow resistance in compound cross-section channels have been investigated by many authors (Huthoff et al. 2008; Khatua and Patra 2007; Mohaghegh and Kouchakzadeh 2008).

Flow velocity is an important hydraulic parameter when we consider overbank flow. When floodplains are inundated, the momentum transfer between the floodplains and the main channel would be strong (Al-Khatib et al. 2012). Thus, the velocity profiles are changed in both the floodplains and the main channel (Knight and Shino 1996; Myers and Lyness 1997; Patra and Kar 2000; Sahu et al. 2011). As a result, it is necessary to provide an effective method for modeling the velocity distribution. To predict the lateral distributions of the depth-averaged velocity in compound channels, many investigators have proposed several methods, such as the numerical simulation (Krishnappan and Lau 1986), experimental research (Yang et al. 2007), and analytical models (Ervine et al. 2000; Huai et al. 2008; Kumar et al. 2005). In engineering practice, analytical models are widely used for simplicity.

Because of the difficulty in obtaining sufficiently accurate and comprehensive field measurements of shear stress and velocity in compound channels (Bhattacharya and Kar 1995; Yang et al. 2012), considerable reliance must still be placed on well-focused laboratory investigations to provide the information concerning the details of the flow structure and the lateral momentum transfer. Such details are important in the development and application of numerical models aimed at solving certain practical open channel flow problems (Khatua et al. 2012; Knight et al. 2007; Tang and Knight 2008).

The aim of this study was to describe the effect of the interaction mechanism on the velocity distribution in a channel of asymmetric compound cross-section (one side floodplain) and to generalize the velocity distribution. In addition, the effect of the height of the flood plain above the main channel bed (step height) and the main channel width on the variation of velocity distribution in both the main channel and the floodplain channel for a given depth ratio of the floodplain to the main channel, h_f/h, is investigated.

2. Experimental apparatus and procedure

The experiments were carried out in a glass-walled smooth laboratory flume 7.5 m long, 0.30 m wide, and 0.3 m deep with a bottom slope of 0.0025 at the fluid mechanics laboratory, Mechanical Engineering Department, Birzeit University, Palestine. The discharge was measured volumetrically with a flow meter with 0.1 l accuracy. A point gauge was used along the centerline of the flume for head measurements. All depth measurements were done with respect to the bottom of the flume. A Pitot tube of circular section with external diameter of 8 mm was used to measure the static and total pressures which were used for the velocities at the required points in the experiments conducted throughout this study.

*Corresponding author. Email: ikhatib@birzeit.edu

The geometries of asymmetric rectangular compound cross-sections were manufactured from Plexiglas and placed at about mid-length of the laboratory flume as symmetric channels have been investigated widely in literature compared to asymmetric channels. In addition, in the nature, the number of asymmetric channels is more than the symmetric ones. The structure of the flow in both of the channels is significantly different. Therefore, we considered only asymmetric channels in this study. Figure 1 shows the plan view and cross-section of the geometries with symbols designating important dimensions of the model elements. The dimensions of the various geometries used in the experiments are given in Table 1. In this study, the model types tested are denoted by MI ($I = 1$–9). Here, B and Z are the width and the step height of the main channel of the asymmetric compound cross-section, respectively.

The required experiments first were conducted in the geometries of the smallest B (= 10 cm) with varying Z values (=2, 4, and 6 cm) and then B was increased to 15 cm at the required amount of Z (=2, 4, and 6 cm), and finally for $B = 20$ cm with the same three values of Z. The entrance angles, θ_1 and θ_2, were 26.565 and 153.35 degrees, respectively. The transition length was twice of the floodplain width, B_f. The recommended entrance angles, θ_1 and θ_2 were experimentally validated, and it was found that these two angles give the smoothest water surface profiles along the models tested compared to others and can be assumed as an acceptable value for practical point of view (Al-Khatib 1993).

In order to determine the velocity distribution in the rectangular compound cross-sections, the channel cross-section was divided by a number of successive lines normal to the direction of the flow. Then the total and static heads were measured at several points along these normal lines by the use of Pitot (Preston) tube. More points were taken close to the channel boundary. Towards the free surface, the distances between the points where the velocities measured were increased. This was done because flow boundary affects the velocity profiles over the flow depth more in the zones close to the boundary than those away from the boundary. Therefore, in order to get reliable velocity profiles over the flow depths, more points were taken close to the channel boundary. Figure 2 shows a definition sketch for the vertical lines over which the velocity measurements were made in the geometries of model types MI, ($I = 1 - 9$).

Numerical integration was used for the calculation of the average main channel velocity (V_{mc}), average floodplain velocity (V_f), and the full cross-sectional velocity (V) for the asymmetrical rectangular compound cross-sections. The cross-sectional area (A) of the channel was divided into (i) number of elementary areas. For each elementary area (ΔA_i),

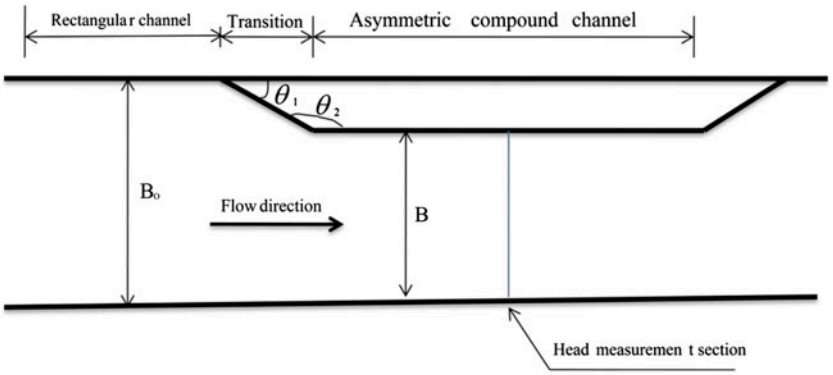

(a) Plan view

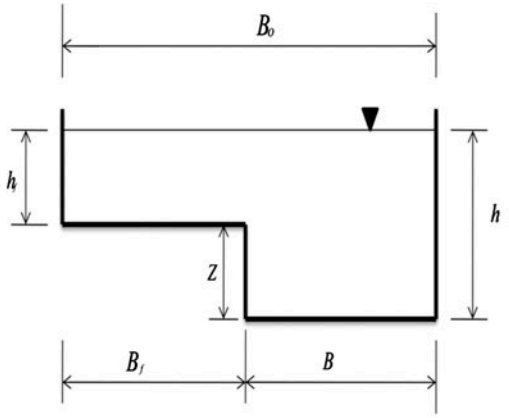

(b) Cross-section of the asymmetric rectangular compound channel

Figure 1. Definition sketch of the flume used in the experiments.

Table 1. Geometrical properties of the asymmetric compound channel geometries.

Types of geometries	B (cm)	Z (cm)	B_f (cm)	B_o/B_f (–)	B_o/Z (–)	B_o/B (–)	B_f/Z (–)	B_f/B (–)	B/Z (–)	h range (cm)	h_f range (cm)	h_r range (–)
M1	10	2	20	1.50	15.00	3.00	10.00	2.00	5.00	4.9–11.0	2.9–9.0	0.59–0.82
M2	10	4	20	1.50	7.50	3.00	5.00	2.00	2.50	6.4–12.1	2.4–8.1	0.39–0.67
M3	10	6	20	1.50	5.00	3.00	3.33	2.00	1.67	8.2–13.6	2.2–7.6	0.27–0.56
M4	15	2	15	2.00	15.00	2.00	7.50	1.00	7.5	5.5–11.4	3.5–9.4	0.64–0.82
M5	15	4	15	2.00	7.50	2.00	3.75	1.00	3.75	6.5–11.1	2.5–7.1	0.38–0.64
M6	15	6	15	2.00	5.00	2.00	2.50	1.00	2.5	7.1–12.1	1.1–6.1	0.15–0.50
M7	20	2	10	3.00	15.00	1.50	5.00	0.50	10.00	4.7–11.2	2.7–9.2	0.57–0.80
M8	20	4	10	3.00	7.50	1.50	2.50	0.50	5.00	5.6–11.4	1.6–9.4	0.29–0.63
M9	20	6	10	3.00	5.00	1.50	1.67	0.50	3.33	7.4–12.3	1.4–6.3	0.19–0.51

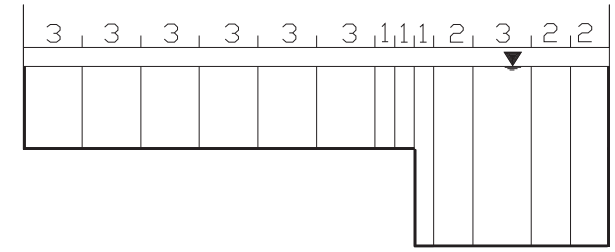

(a) MI Model types, I = 1, 2, 3

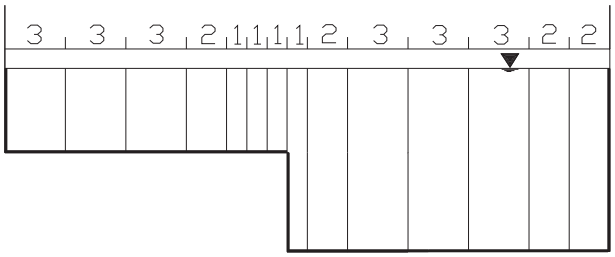

(b) MI Model types, I = 4, 5, 6

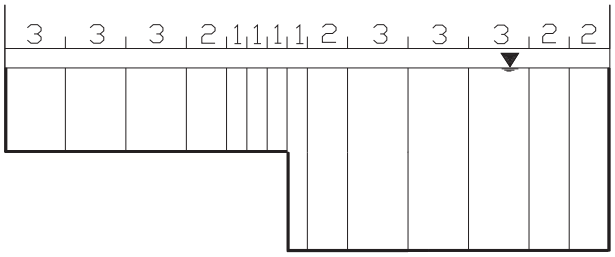

(c) MI Model types, I = 7, 8, 9

Figure 2. Definition sketch for vertical lines over which velocity measurements were made for the different geometries, (dimensions are in cm).

the corresponding average velocity (u_i) was determined from the measured velocities. The cross-sectional average velocity (U) was calculated using Equation (1) (Al-Khatib 2013).

$$U = \frac{\sum_{i=1}^{N} u_i \Delta A_i}{A} \tag{1}$$

3. Presentation and discussion of results

Velocity distribution patterns were obtained for different depths of flow, each corresponding to certain step height only, while the others were within the full cross-section related to the geometry of each model.

3.1. *Variation of velocity ratios V_f/V, V_{mc}/V, V_{mc}/V_f with the relative depth*

Ratios of average main channel velocity (V_{mc}) and average floodplain velocity (V_f) to full cross-sectional velocity (V) as a function of the relative depth, h_r which equals to h_f/h ratio, where h_f = floodplain water depth; h = main channel water depth are shown in Figures 3–8. From these figures, it is clearly seen that as the relative depth, h_r, increases, V_f/V values increase up to a certain value of h_r and then become almost constant ($0.19 \le h_r \le 0.79$; $1.5 \le B_O/B \le 3.0$; $5 \le B_O/Z \le 15$; $1.5 \le B_O/B_f \le 3.0$) while V_{mc}/V values very slightly decrease. This applies for all models except model M7 (Figure 6) where, V_f/V value first decreases with increasing h_r and then increases, and V_{mc}/V values very slightly decrease with increasing h_r to a certain point then decrease. V_{mc}/V ratio is less than V_f/V for small B values (Geometries M1, M2, and M3) then becomes greater than V_f/V for geometries with large B values (Geometries M7, M8, and M9) used in the experiments.

Figures 3 and 4 belongs to the models M1 and M2 for which $B = 10$ cm in both of them and $Z = 2$ and 4 cm, respectively. Since in these two models the width of the floodplain is the maximum, $B_f = 20$ cm, and the step heights $Z = 2$ and 4 cm, when the flow occurs through the channel, the discharge of the floodplain is larger than that of the main channel. Therefore, V_f/V is larger than V_{mc}/V. We have reverse situation in Figures 6 and 7 where the models are M7 and M8, the main channel width is maximum, $B = 20$ cm, in both of them and the floodplain width is the minimum, $B_f = 10$ cm. Most of the flow occurs through the main channel so V_{mc}/V is larger than V_f/V.

For the same B_0/B ratio, velocity distribution trend gets changed at higher depths for M3 and M9 (Figures 5 and 8). The reason for that is the step height. This situation is clearly seen from Figures 3–8; for the models of $B_0/B = 3.0$ (M1, M2, and M3) and $B_0/B = 1.5$ (M7, M8, and M9) for which B and B_f values are the same and the only difference is on Z values; $Z = 2$, 4, and 6 cm, respectively. It is obvious that as the flow depth increases in the channel, the rate of increase of the flow depth in the main channel becomes less than the rate of increase of the flow depth in the flood plain, especially for the channels of large Z values as $Z = 6$ cm. In this case, the water area in the floodplain increases much faster than that of the main channel. Therefore, the increase in the floodplain discharge becomes much more than that of the main channel which results in increase in the value of V_f/V while the value of V_{mc}/V does not change too much. For the channels of small Z values ($Z = 2$ cm) and large B values ($B = 20$ cm), the reverse of this process occurs while the flow depth increasing in the channel (Figure 6). For channels of $Z = 2$ cm and $B_0 = 10$ cm, Model M1, V_{mc}/V increases with increasing h_r while V_f/V decreases (Figure 3).

In order to see the effect of the main channel bottom width, B, and the step height, Z, on the variation of h_r with V_{mc}/V, V_{mc}/V, Figures 9–11 were plotted.

Figures 9 and 10 show the variation of the cross-sectional velocities, V_f/V, V_{mc}/V, with the relative depth h_r. From these figures, one can say that for a given h_r, the ratio of V_f/V increases as the B_O/B ratio increases. And this ratio also increases as the step height, Z, increases, in most of the geometries ($0.15 \le h_r \le 0.82$; $1.5 \le B_O/B \le 3.0$; $0.5 \le B_f/B \le 2.0$; $1.5 \le B_O/B_f \le 3.0$). Also as it was mentioned before, V_f/V as h_r values increase, the V_f/V ratio increases up to a certain value and then it becomes almost constant. V_f/V values are always less then unity except for the geometries with small B values (M1, M2, and M3). In this situation, the momentum transfer is from the floodplain to the main channel for these geometries. For h_r values above 0.55 for almost all geometries, V_f/V values become constant (Figure 9). V_{mc}/V values decrease as h_r values increase (Figure 10). For geometries with $0.15 \le h_r \le 0.81$; $2.0 \le B_O/B \le 3.0$; $0.5 \le B_f/B \le 1.0$; $2 \le B_O/B_f \le 3.0$, V_{mc}/V is greater than unity for almost all h_r values. This situation confirms that the momentum transfer is from the main channel to the floodplain.

We had also mentioned that V_{mc}/V ratio was a function of the relative depth, h_r. So that for a constant h_r value, the ratio of V_{mc}/V increases as the main channel width, B, decreases, and it also increases as the step height, Z, increases for

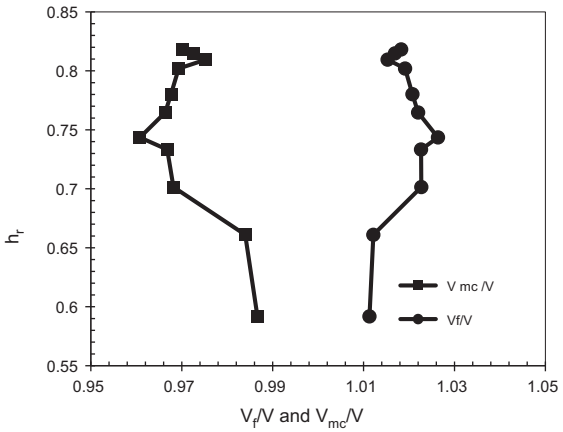

Figure 3. Variation of cross-sectional velocities with the relative depth, h_r, for model M1 ($B_0/B = 3.0$).

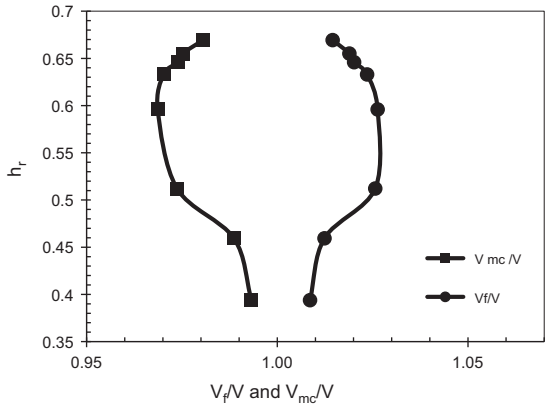

Figure 4. Variation of cross-sectional velocities with the relative depth, h_r, for model M2 ($B_0/B = 3.0$).

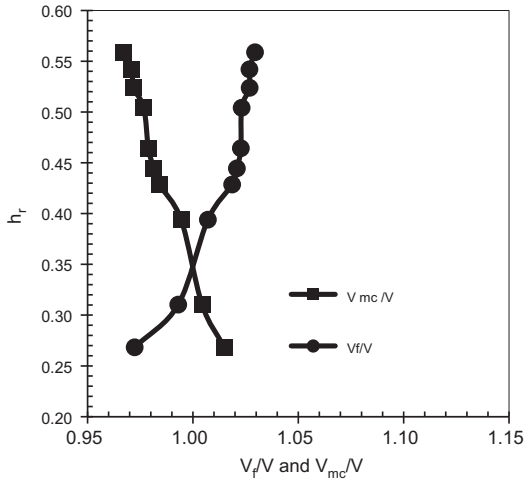

Figure 5. Variation of cross-sectional velocities with the relative depth, h_r, for model M3 ($B_0/B = 3.0$).

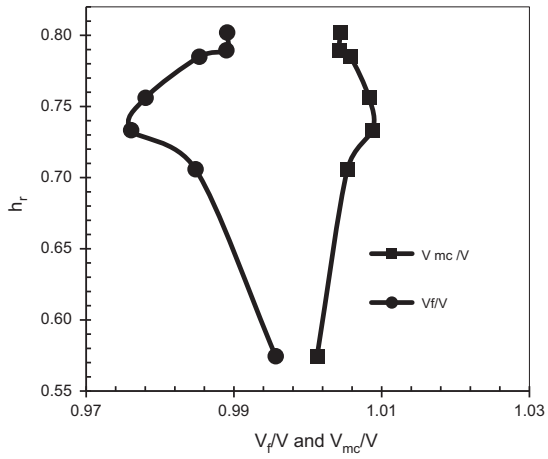

Figure 6. Variation of cross-sectional velocities with the relative depth, h_r, for model M7 ($B_0/B = 1.5$).

almost all the geometries. As the main channel width, B, increases, V_{mc}/V ratio tends toward unity as seen from the curves of geometries M7, M8, and M9 which have the largest main channel widths (Figure 10). The ratios of the main channel to floodplain velocity, V_{mc}/V_f are shown in Figure 11. From this figure, it is clearly shown that as the main channel width, B, for the different geometries, increases, the velocity ratio V_{mc}/V_f increases. The reverse situation occurs as the step height,

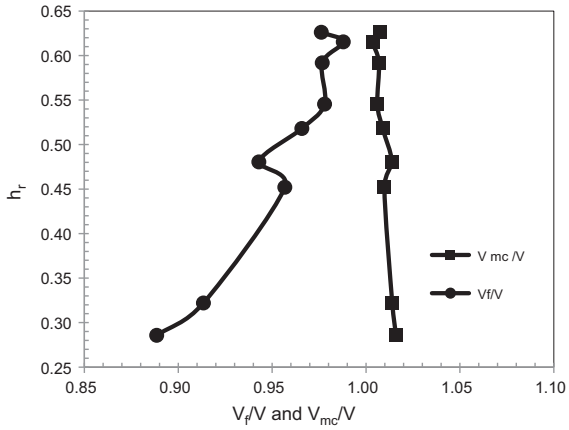

Figure 7. Variation of cross-sectional velocities with the relative depth, h_r, for model M8 ($B_0/B = 1.5$).

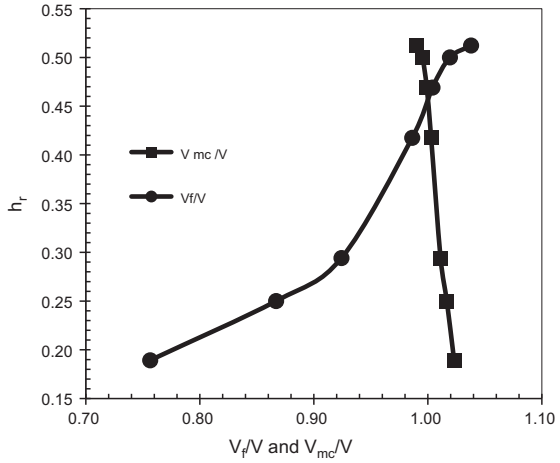

Figure 8. Variation of cross-sectional velocities with the relative depth, h_r, for model M9 ($B_0/B = 1.5$).

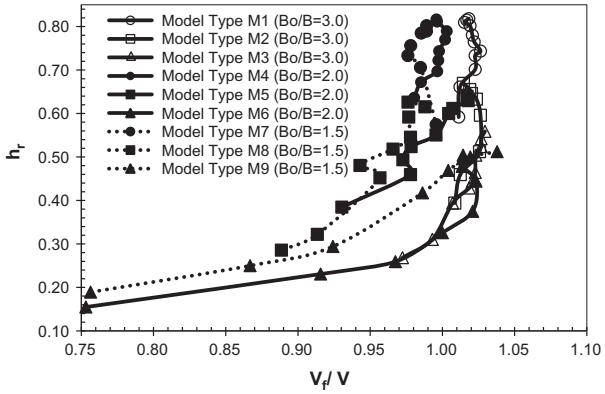

Figure 9. Depth variation of ratios of main channel to cross-sectional velocities for different geometries.

Z, increases for the same B value while h_r is kept constant. This is due to having higher rate of increase of V_f/V with increasing Z (Figure 9) than the rate of decrease of V_{mc}/V with increasing Z (Figure 10) for a given h_r value. It can also be seen that the V_{mc}/V ratio is always greater than unity for intermediate and large B values ($2.0 \le B_O/B \le 3.0$; $0.5 \le B_f/B \le 1.0$; $2 \le B_O/B_f \le 3.0$), and tends toward less than unity for small B values. This result explains the momentum transfer from main channel to floodplains for small floodplain width and the opposite for large floodplain width. For the cross-sections of which h_r are about less than 0.35, the value of V_{mc}/V is always larger than unity, and therefore, in all these cases the momentum is transferred from the main channel to the floodplains.

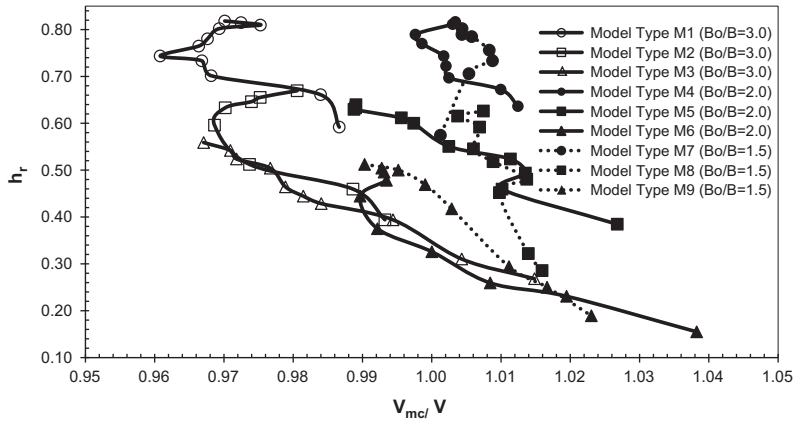

Figure 10. Depth variation of ratios of main channel to cross-sectional velocities for different geometries.

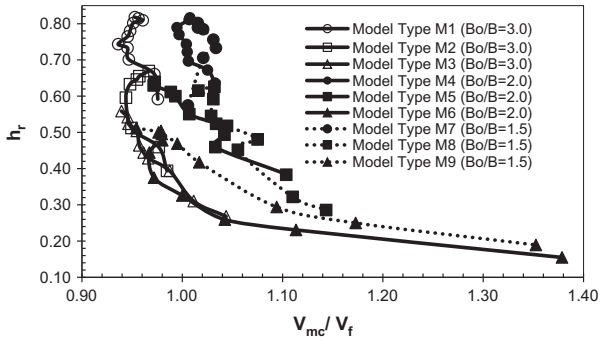

Figure 11. Depth variation of velocities ratio for different cross-sections.

3.2. *Generalization of the variation of velocity ratios of V_f/V, V_{mc}/V, V_{mc}/V_f with the relative depth*

A generalized single variable regression model has been derived to predict each of the three dimensionless velocity ratios of V_f/V, V_{mc}/V, and V_{mc}/V_f as a function of the relative depth (h_r). The prediction model is power in form as indicated by Equations (2)–(4). The linear multiple-variable regression techniques have been used to estimate the regression coefficients associated with the model after performing the necessary linear transformation.

$$\frac{V_f}{V} = C(h_r)^c \tag{2}$$

$$\frac{V_{mc}}{V} = D(h_r)^d \tag{3}$$

$$\frac{V_{mc}}{V_f} = K(h_r)^k \tag{4}$$

Table 2 provides the derived numerical values of the regression parameters (C, c; D, d; K, k) for a total of 27 different geometries representing three types of dimensionless velocity ratios for each of the nine different asymmetric compound cross-section cases. The derivation of the generalized model provided in Equations (2)–(4) has been accomplished based on the optimization of the correlation coefficient (r), which has been maximized to very high values, which for a line of perfect would have a value of ±1. In addition, the average correlation coefficient is given in Table 2. As a general trend, as the Z value increases for constant B value, the r value increases.

Most of the obtained statistics indicate that the derived regression geometries are powerful and can effectively be used to estimate the dimensionless velocity ratios with a high degree of reliability for constructed asymmetric compound cross-sections based only on the relative depth. Therefore, the derived general power model presented in Equations (2)–(4) is an appropriate model to be used in predicting the dimensionless velocity ratios in open channels of asymmetric rectangular compound cross-sections. The model regression parameters (C, c; D, d; K, k) need to be estimated for any particular cross-section geometry since Table 2 indicates that these coefficients are different for each compound cross-section type.

Table 2. Values of the exponent, coefficient and correlation coefficient of the relationship given by Equations (2)–(4).

Exponent, coefficient and r	Types of geometries									Average value of r
	M1	M2	M3	M4	M5	M6	M7	M8	M9	
c	0.112	0.060	0.077	0.110	0.173	0.275	−0.131	0.130	0.298	0.773
C	1.053	1.055	1.082	1.029	1.101	1.299	0.946	1.050	1.277	
r	0.402	0.539	0.973	0.783	0.977	0.887	0.451	0.973	0.976	
d	−0.126	−0.061	−0.065	−0.074	−0.079	−0.041	0.041	−0.017	−0.031	0.827
D	0.936	0.944	0.932	0.981	0.956	0.959	1.018	0.997	0.974	
r	0.620	0.760	0.993	0.750	0.964	0.954	0.543	0.879	0.982	
k	−0.238	−0.121	−0.142	−0.184	−0.252	−0.316	0.172	−0.147	−0.329	0.809
K	0.889	0.895	0.861	0.953	0.868	0.738	1.076	0.950	0.763	
r	0.544	0.677	0.989	0.771	0.976	0.901	0.476	0.969	0.981	

The measured dimensionless velocity ratios and the predicted ones by utilizing Equations (2)–(4) are plotted for two selected cross-sections (M5 and M9) as shown in Figures 12 and 13. As seen from these two figures, the values of the measured and predicted dimensionless velocity ratios are very close to each other. Using the procedure described, the dimensionless velocity ratios in asymmetric rectangular compound cross-sections with $1.5 \le B_O/B_f \le 3.0$; $5.0 \le B_O/Z \le 15.0$; $1.5 \le B_O/B \le 3.0$; $1.67 \le B_f/Z \le 10.0$; $0.5 \le B_f/B \le 2.0$; $5.0 \le B/Z \le 3.33$ have been estimated with high accuracy with maximum errors of about 7, 2, and 9%, and the mean errors of 1.2, 0.4, and 1.5% for V_f/V, V_{mc}/V, *and* V_{mc}/V_f, respectively. These error percentages were obtained by introducing the measured and predicted dimensionless velocity ratios with independent data-sets (data which were not used in derivation of the relationships) for a given h_r value in Equation (5).

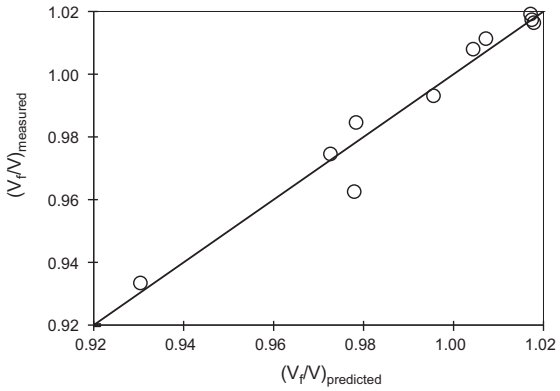

Figure 12. Measured vs. predicted V_f/V ratio for Model M5.

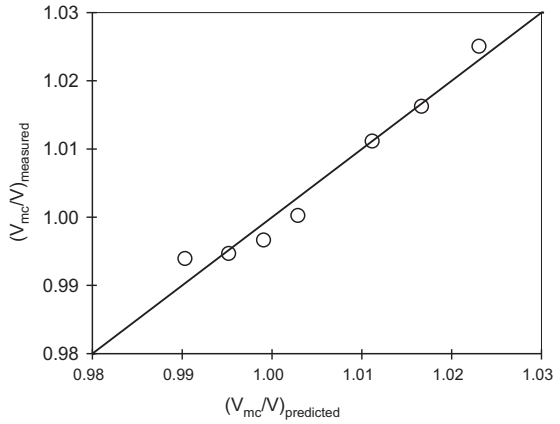

Figure 13. Measured vs. predicted V_{mc}/V ratio for model M9.

Table 3. Numerical example of the dimensionless velocity ratios for Model M3.

h_r	$\left(\frac{V_f}{V}\right)_{calculated}$	$\left(\frac{V_f}{V}\right)_{predicted}$	$\lvert Error_1\rvert$ (%)	$\left(\frac{V_mc}{V}\right)_{calculated}$	$\left(\frac{V_mc}{V}\right)_{predicted}$	$\lvert Error_2\rvert$ (%)	$\left(\frac{V_mc}{V_f}\right)_{calculated}$	$\left(\frac{V_mc}{V_f}\right)_{predicted}$	$\lvert Error_3\rvert$ (%)
0.5588	1.0295	1.0342	0.4603	0.9671	0.9681	0.1029	0.9394	0.9352	0.0045
0.5420	1.0268	1.0318	0.4811	0.9709	0.9700	0.0972	0.9456	0.9392	0.0067
0.5238	1.0269	1.0290	0.2062	0.9718	0.9721	0.0348	0.9463	0.9438	0.0027
0.5041	1.0231	1.0260	0.2800	0.9767	0.9746	0.2183	0.9546	0.9489	0.0059
0.4643	1.0227	1.0195	0.3213	0.9789	0.9798	0.0929	0.9571	0.9601	0.0031
0.4444	1.0209	1.0160	0.4741	0.9815	0.9826	0.1130	0.9614	0.9661	0.0049
0.4286	1.0186	1.0132	0.5348	0.9840	0.9849	0.0855	0.9661	0.9711	0.0052
0.3939	1.0071	1.0066	0.0522	0.9944	0.9903	0.4155	0.9874	0.9828	0.0047
0.3103	0.9930	0.9881	0.4920	1.0043	1.0058	0.1417	1.0114	1.0166	0.0052
0.2683	0.9724	0.9771	0.4843	1.0148	1.0153	0.0464	1.0437	1.0379	0.0054

$$\text{Error}\% = \left[\frac{(\text{velocity ratio})_{measured} - (\text{velocity ratio})_{predicted}}{(\text{velocity ratio})_{measured}}\right] \times 100\% \tag{5}$$

Numerical Example

The model M3 yielded high correlation coefficients for the three different dimensionless velocity ratios. In this numerical example, the use of the recommended model type is described; eventually, the total error in the estimation of the three different dimensionless velocity ratios is determined using the related tables and equations. In Table 3 in a row, some of the dimensionless velocity ratios calculated from the results of the experiments, $\left(\frac{V_f}{V}_{measured}\right)$, $\left(\frac{V_{mc}}{V}_{measured}\right)$ and $\left(\frac{V_{mc}}{V_f}_{measured}\right)$ and h_r are given for model M3. As can be seen from this table, the maximum amount of the absolute error for the three dimensionless ratios is less than 1%. Equations (2)–(4) are general equations and can be used with exponents and coefficients presented in Table 2 to estimate the dimensionless velocity ratios in asymmetric compound cross-sections with similar geometries.

3.3. *Multiple-variable regression prediction models*

A generalized multiple-variable regression model has been derived to predict each of the three experimentally measured dimensionless velocity ratios as a function of two dimensionless parameters which are the relative depth (h_r) and B_0/B. The prediction models are in the forms indicated by Equations (6–8).

$$V_1 = a_1 + b_1 h_r + b_2[\log_{10}(h_r) \times (h_r)^{0.45}] + d_1[\log_{10}(h_r) \times (h_r)^{0.45}] \times \left(\frac{1}{W}\right)^{1.7} \tag{6}$$

$$V_2 = a_1 + b_1 h_r + c_1 W + d_1\left[\log_{10}(h_r) \times \left(\frac{W-1}{W}\right)^{0.5}\right] \tag{7}$$

$$V_3 = a_1 + b_1 h_r + b_2[\log_{10}(h_r) \times (h_r)^{0.45}] + c_1 W \tag{8}$$

where $V_1 = \frac{V_{mc}}{V}^{-0.99}$, $V_2 = \frac{V_{mc}}{V}$, $V_3 = \left(\frac{V_{mc}}{V_f}\right)^{3.2}$, $W = \frac{B_0}{B}$, $h_r = \frac{h_f}{h}$, a_1 = regressions' constant; and b_1, b_2, c_1, and d_1 = regressions' coefficients.

According to Equations (6–8), a multiple-variable predictive model can be derived for each dimensionless velocity ratio resulting in three different regression models. Therefore, the velocity measurements estimated for a particular mean velocity type as obtained from the nine different compound cross-section types will be pooled together for the purpose of developing one multiple-variable regression model for each average dimensionless velocity ratio. Although the relationship between the dependent variables and the independent variables in Equations (6–8), is a non-linear one, the equations are linear in terms of the coefficients, hence, the linear multiple-variable regression techniques can be applied which are mainly dependent on the minimization of the sum of squared errors.

Table 4 provides the derived regression parameters (a_1, b_1, b_2, c_1, and d_1) for the three dimensionless velocity ratios. The R^2 has ranged from 0.829 to 0.888 which can be considered relatively high. This can be attributed to using more variables in the multiple-variable regression models and to the non-homogeneity of the data used to develop the multiple-variable models.

Table 4. Regression coefficients and statistics for multiple-variable prediction models.

Statistics	V_1	V_2	V_3
R^2	0.888	0.829	0.883
R^2_{adj}	0.883	0.823	0.878
S_{Vi}	0.02	0.007155	0.11012
CV_{ij}(%)	5.0	1.7	7.5
a_1	7.374	0.974	35.750
b_1	−6.379	0.093	−34.446
b_2	14.698	–	78.257
c_1	–	−0.032	−0.153
d_1	−0.689	−0.051	–
t_{b1}	−17.420	5.235	−17.747
t_{b2}	17.274	–	17.295
t_{c1}	–	−14.755	−7.611
t_{d1}	−8.374	−7.490	–
Sample size	80	80	80

The same notice and explanation apply to the second main statistic, namely, the coefficients of variation (CV) wherein their values are acceptable with values below 10% (1.7–5.0%). The lower the CV, the smaller the residuals relative to the predicted value. This is suggestive of a good model fit. The third main statistic is the student t-value associated with the independent variable coefficients (b_1, b_2, c_1, and d_1). The corresponding t-values have been maximized to reflect a confidence level exceeding 99.9% which reflects a very high level of reliability in the predictive strength of the developed models. Hence, it can be concluded that the regression models developed for the three dimensionless velocity ratios fit the data very well. Finally, the generated regression models were validated using a holdout sample of about 50% of the total sample size (i.e. 40 observed dimensionless velocity ratio measurements) to verify the models' predictive strength. The corresponding mean of the squared prediction errors (MSPR) was calculated for each model with the results provided in Table 5. It is clear from Table 5 that the MSPR values, as obtained from Equation (9), are close to their corresponding mean squared errors (MSE) for the three predictive models. This means that the MSE statistic was not seriously biased and it provided an appropriate indication of the predictive ability of the derived models (Kutner et al. 2005).

$$\text{MSPR} = \frac{\sum_{i=1}^{n*} (Y_i - \hat{Y}_i)}{n*} \tag{9}$$

Table 5. MSE and MSPR associated with the three multiple-variable regression models.

Dependent variable	MSE	MSPR
V_1	0.00043	0.00035
V_2	0.00005	0.00004
V_3	0.01213	0.01175

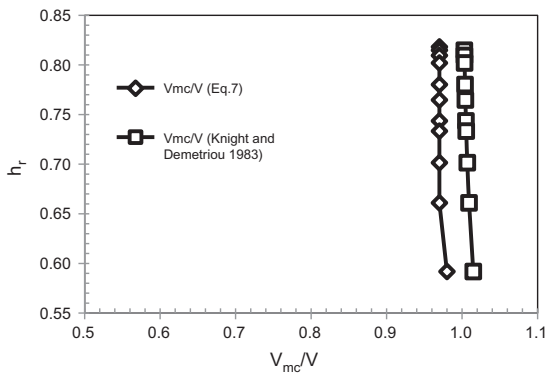

Figure 14. Comparison of h_r vs. V_{mc}/V of present results (Equation (7)) with those of Knight and Demetriou (1983) for model M1.

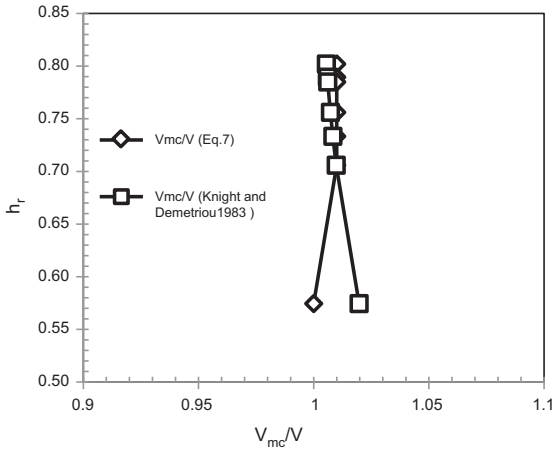

Figure 15. Comparison of h_r vs. V_{mc}/V of present results (Equation (7)) with those of Knight and Demetriou (1983) for model M7.

where: Y_i = the value of the response variable in the ith validation case, $\hat{Y}_i$ = the predicted value for the ith validation case based on the model-building data-set, and n^* = the number of cases in the validation data-set.

For the sake of comparison of the present results, the data of Knight and Demetriou (1983) who investigated a smooth symmetrical rectangular compound channel having a bank full depth of 7.5 cm, and two floodplains 22.9 cm wide with a constant bed slope of 0.000966 are utilized. They presented the following equation for the ratio of the main channel to the average compound section velocity, V_{mc}/V:

$$\frac{V_{mc}}{V} = 1.0 + 1.08[(W-1)h_r + 1]\left[\frac{W-1}{W}\right]^{0.25}(3.3h_r)^{4/W}e^{-9.9h_r} \tag{10}$$

where $W = Bo/B$, and e = base of natural logarithm.

This equation was plotted in Figures 14 and 15 to compare the V_{mc}/V ratios given by this equation with those calculated by Equation (7). The analysis of the aforementioned figures shows that Equation (10) a little bit overestimates or coincides with the V_{mc}/V ratio presented by Equation 6. The calculted error between the valus presented by Equations (7) and (10) ranged between 0.4 and 6.1% with a mean value of 2.8%.

4. Conclusions and recommendations

The present paper analyzed the velocity distribution in an asymmetrical compound channel with nine different geometries through conducting a series of laboratory experiments. The following conclusions can be drawn.

(1) For a given h_r, the ratio V_f/V increases as the step height, Z, increases. This ratio increases as the main channel width, B, decreases.
(2) For a constant h_r value, the ratio V_{mc}/V decreases as step height, Z, increases, and it increases as the main channel width, B, decreases.
(3) As the main channel width, B, for the different geometries, increases, the velocity ratio V_{mc}/V_f increases. The reverse situation occurs as the step height, Z, increases for the same B value while h_r is kept constant.
(4) The derived general power model presented in Equations (2)–(4) is an appropriate model to be used in predicting dimensionless velocity ratios in open channels of asymmetric rectangular compound cross-sections with high accuracy in such a way that regardless of the model type, these equations can be used to predict velocity ratios within the range of flow conditions examined in this study.
(5) The dimensionless velocity ratio measurements for the nine different compound cross-section configurations were plotted together for the purpose of generating a multiple-variable regression model for each dimensionless velocity ratio. Three distinct multiple-variable predictive models were obtained as a function of two dimensionless dependent parameters which are h_r and B_0/B. The same three main statistics outlined earlier have indicated that the derived multiple-variable predictive models are quite reliable. Additional model validation was done including the normal probability plots, residual plots, and MSPR. These validation measures have all indicated the appropriateness of the derived models in predicting the three dimensionless mean flow velocities.

Nomenclature

The following symbols are used in this paper:

a_1	regressions' constant
B	bottom width of the approach channel;
B_f	floodplain channel width;
B_o	bottom width of the upstream channel;
b_1, b_2, c_1, and d_1	regressions' coefficients;
C, c	coefficient and exponent used in Equation (7)
D, d	coefficient and exponent used in Equation (8)
e	base of natural logarithm;
g	gravitational acceleration;
h_f	floodplain water depth;
h	main channel water depth;
h_r	relative depth which equals to h_f/h ratio;
K, k	coefficient and exponent used in Equation (9)
n^*	the number of cases in the validation data-set;
Q	volume rate of flow;
r	correlation coefficient;
V	average full cross-sectional streamwised flow velocity;
V_f	average streamwised flow velocity in the floodplain;
V_1	$\left(\frac{V_f}{V}\right)^{-0.99}$
V_2	$\frac{V_{mc}}{V}$
V_3	$\left(\frac{V_{mc}}{V_f}\right)^{3.2}$
W	Bo/B
Y_i	the value of the response variable in the ith validation case
$\hat{Y}_i$	the predicted value for the ith validation case based on the model-building data-set
Z	height of the flood plain above the main channel bed (step height)
θ_1 and θ_2	entrance angles

References

Al-Khatib, I.A. (1993). "Hydraulic characteristics and optimum design of symmetrical compound channels for flow measurements." Ph.D. dissertation, Middle East Tech. Univ., Ankara, Turkey.

Al-Khatib, I.A. (2013). "Investigation of momentum and kinetic energy correction coefficients in asymmetric compound cross section flumes." *Turk. J. Eng. Envıron. Scı.*, 37, 69–78.

Al-Khatib, I.A., Dweik, A.A., and Gogus, M. (2012). "Evaluation of separate channel methods for discharge computation in asymmetric compound channels." *Flow Meas. Instrum.*, 24, 19–25.

Al-Khatib, I.A., Hassan, H., and Abaza, K.A. (2013). "Application and validation of regression analysis in the prediction of discharge in asymmetric compound channels." *J. Irrigat. Drain. Eng.*, 139(7), 542–550.

Bhattacharya, A.K., and Kar, S.K. (1995). "A model for the stage-discharge relationship in compound open channels." *ISH J. Hydraul. Eng.*, 1(2), 59–62.

Ervine, D.A., Babaeyan-Koopaei, K., and Sellin, R.H.J. (2000). "Two-dimensional solution for straight and meandering overbank flows." *J. Hydraul. Eng.*, 126(9), 653–669.

Huai, W., Xu, Z., Yang, Z., and Zeng, Y. (2008). "Two dimensional analytical solution for a partially vegetated compound channel flow." *Appl. Math. Mech.*, 29(8), 1077–1084.

Huthoff, F.P.C., Roos, Pieter C., Augustijn, D. C. M., and Hulscher, S. J. M. H. (2008). "Interacting divided channel method for compound channel flow." *J. Hydraul. Eng.*, 134(8), 1158–1165.

Khatua, K.K., and Patra, K.C. (2007). "Boundary shear stress distribution in compound open channel flow." *ISH J. Hydraul. Eng.*, 13 (3), 39–54.

Khatua, K.K., Patra, K.C., and Mohanty, P.K. (2012). "Stage-discharge prediction for straight and smooth compound channels with wide floodplains." *J. Hydraul. Eng.*, 138(1), 93–99.

Knight, D.W., and Demetriou, J.D. (1983). "Flood plain and main channel flow interaction." *J. Hydraul. Eng.*, 109(8), 1073–1092.

Knight, D.W., and Shino, K. (1996). "River channel and floodplain hydraulics." *Floodplain processes*, M.G. Anderson, D.E. Walling, and P.D. Bates, eds., John Wiley and Sons, Chichester, 139–182.

Knight, D.W., Omran, M., and Tang, X. (2007). "Modeling depth-averaged velocity and boundary shear in trapezoidal channels with secondary flows." *J. Hydraul. Eng.*, 133(1), 39–47.

Krishnappan, B.G., and Lau, Y.L. (1986). "Turbulence modeling of flood plain flows." *J. Hydraul. Eng.*, 112(4), 251–266.

Kumar, A., Samaiya, N.K., and Kothyari, U.C. (2005). "Velocity, discharge and turbulence characteristics in a straight compound channel." *ISH J. Hydraul. Eng.*, 11(3), 91–102.

Kutner, M., Nachtsheim, C., Neter, J., and Li, W. (2005). *Applied linear statistical models*, McGraw-Hill/Irwin, New York, NY.

Mohaghegh, A., and Kouchakzadeh, S. (2008). "Evaluation of stage-discharge relationship in compound channels." *J. Hydrodyn. Ser. B*, 20(1), 81–87.

Myers, R.C., and Lyness, J.F. (1997). "Discharge ratios in smooth and rough compound channels." *J. Hydraul. Eng.*, 123(3), 182–188.

Patra, K.C., and Kar, S.K. (2000). "Flow interaction of meandering river with floodplains." *J. Hydraul. Eng.*, 126(8), 593–604.

Sahu, M., Khatua, K.K., and Mahapatra, S.S. (2011). "A neural network approach for prediction of discharge in straight compound open channel flow." *Flow Meas. Instrum.*, 22, 438–446.

Tang, X., and Knight, D.W. (2008). "A general model of lateral depth-averaged velocity distributions for open channel flows." *Adv. Water Res.*, 31(5), 846–857.

Yang, K., Cao, S., and Knight, D.W. (2007). "Flow patterns in compound channels with vegetated floodplains." *J. Hydraul. Eng.*, 133 (2), 148–159.

Yang, Z., Gao, W., and Huai, W. (2010). "Secondary flow coefficient of overbank flow." *Appl. Math. Mech.*, 31(6), 709–718.

Yang, Z., Gao, W., and Huai, W. (2012). "Estimation of discharge in compound channels based on energy concept." *J. Hydraul. Res.*, 50 (1), 105–113.